*machines*

MDPI

*Article*

# Modeling and Analysis of Clutch Nonlinear Behavior in an Automotive Driveline for Suppressing Torsional Vibration

**Junlong Qu [1], Wenku Shi [1], Juncheng Wang [2] and Zhiyong Chen [1,*]**

[1] College of Automotive Engineering, Jilin university, Changchun 130022, China
[2] BAIC Foton Automobile Co., Ltd., Zhucheng 262233, China
* Correspondence: chen_zy@jlu.edu.cn

**Abstract:** Torsional vibration of the automotive driveline has significant influence on driving comfort. This study investigates the influence of clutch nonlinear behaviors on the torsional vibration of the driveline with numerical and experimental methods. A generic automobile powertrain model with 7 degrees of freedom is proposed considering the transient engine torque, the nonlinear characteristics of multi-stage clutch and tire slip. Taking a commercial vehicle as an example, the dynamic behaviors and inherent characteristics of the driveline system are calculated and analyzed. Based on the proposed model, the influences of the clutch parameters on driveline torsional vibration are investigated. In order to validate the proposed model and the analytical results, an optimized clutch is designed and the experiments of torsional vibration are conducted with the prototype and the optimized clutch. The analytical and experimental results demonstrate that an increase in the first end-stop angle and the main-stage hysteresis or a decrease in the second end-stop angle and the main-stage stiffness of the clutch can effectively suppress driveline torsional vibration during vehicle accelerating.

**Keywords:** automotive powertrain; torsional vibration; multi-stage clutch; vibration control; nonlinear



**Citation:** Qu, J.; Shi, W.; Wang, J.; Chen, Z. Modeling and Analysis of Clutch Nonlinear Behavior in an Automotive Driveline for Suppressing Torsional Vibration. *Machines* **2022**, *10*, 819. https://doi.org/10.3390/machines10090819

Received: 23 August 2022
Accepted: 15 September 2022
Published: 18 September 2022



## 1. Introduction

The torsional vibration of a powertrain system has significant influence on drivers' comfort and usually takes place during vehicle accelerating [1,2]. The vibration of the driveline can be transmitted through connecting structures between the chassis and vehicle body, arousing abnormal vibration and booming noise in the cabin [3]. The torsional resonance is usually considered related to the natural frequencies of the driveline between 25 and 100 Hz [4]. When an automobile accelerates from low speed to high speed, it is equivalent to applying an up-sweep frequency excitation to the driveline system [5,6]. During this process, certain driveline components violently vibrate beyond the balance speed if passing through the critical speed [7]. Many researchers have investigated this problem and attribute it to the crude operation of the engine and the undamped driveline system. However, improving engine performance or redesigning the whole drivetrain system will greatly increase development costs, especially when the vehicle is already prototyped. The optimal design of clutch parameters can be an alternative and low-cost approach to mitigating driveline vibration [8,9]. Consequently, it is important to investigate the nonlinear behavior of the clutch and its influence on driveline torsional vibration.

Modeling of the powertrain system has been studied in the past years. Crowther and Zhang [10] modeled the direct, geared, branched, grounded and gear-mesh elements of the driveline and developed a six-degree-of-freedom (6DOF) dynamic model by assembling these elements. They researched the low-frequency transients of clutch engagement stick-slip and gear backlash. To analyze the influence of clutch parameters on gear rattles, Wei [11], Shangguan [12] and Yucesan et al. [13] developed powertrain models including a multi-stage clutch model and a contact model of geared teeth. A nonlinear 4DOF drivetrain

model considering the characteristics of friction clutch was proposed in Ref. [14] for suppressing car starting judder. Wei et al. [11] also discussed the modeling method of transient engine torque in his research, and Rezeka [15] and Wu et al. [16] developed the approach to evaluating the instantaneous friction in internal combustion engines. In Ref. [17], Bartram and Mavros analyzed the effects of road friction on driveline vibration by comparing the simulation results among four different boundary conditions of tires.

Idehara [8] and Liu et al. [9] analyzed the influences of clutch parameters on the torsional vibration of the drivetrain with nonlinear models. They concluded that increasing the friction moment of the clutch could reduce the vibration amplitude of the gearbox, and a decrease in clutch stiffness would lower the natural frequency of the powertrain system. Jurmu [18], Yang [19] and Steinel et al. [20] studied the utilization of torsional vibration absorbers (TVAs) in suppressing vehicle driveline resonance. The nonlinear vibration of a multi-stage clutch damper was analyzed in Refs. [21–24]. They developed simplified single- or double-DOF driveline models with piecewise linear stiffness and hysteresis and calculated the frequency response function of the vibration system through analytical methods, such as the KB method, HBM and IHB. It indicated that when the system had hardening characteristics of stiffness, the amplitude–frequency curve would bend to the right at the transition angle, and the peak amplitude of the resonant region would decrease.

In previous research, the established models usually simplify the nonlinearities so that they cannot precisely capture the transient behaviors of the automobile driveline, and the investigations of clutch parameter influences are mainly concentrated on the stiffness and damping, which does not reveal the effects of end-stops and the cross-area vibration of the clutch damper. This research proposes a generic driveline model considering important nonlinearities of the driveline components and focuses on the influences of clutch nonlinear characteristics on the driveline torsional vibration. The article is organized as follows. Firstly, a generic nonlinear driveline model with 7 degrees of freedom is developed. Taking a light-loaded commercial automobile as an example, the experiment of driveline torsional vibration is set up to validate the model. Then, the dynamic behaviors and natural characteristics of the driveline system are calculated and analyzed with numerical methods. Based on the proposed model, the influences of the clutch parameters on the driveline oscillation are analyzed. According to the analytical results, a revised multi-stage clutch with optimized stiffness and end-stops is designed and tested to validate the analytical results. Finally, conclusions are drawn in Section 7.

## 2. Analytical Model of Powertrain System

### *2.1. Driveline Model*

To investigate the torsional vibration of the powertrain system, a seven-degree-of-freedom (7DOF) nonlinear model is developed, as shown in Figure 1. Here, $J_i$ and $\theta_i$ $i(i = 1, 2, \cdots, 7)$ represent the moments of inertia and the angular displacements of different components, respectively. The subscripts $i(i = 1, 2, \cdots, 7)$ represent the engine, the driving part of clutch, the sum of the driven part of clutch and transmission, driveshafts, the sum of final drive and differential, driving wheels and vehicle body, respectively. The notations $k_s$ and $H$ represent the stiffness and hysteresis of the clutch damper, respectively. The stiffness and viscous damping coefficients of different connecting shafts are represented by $k_{ij}$ and $c_{ij}$ $(i = 3, 4, 5;\ j = i + 1)$, respectively. $T_e$ denotes the transient output torque of engine. $T_c$ is the torque of clutch friction plates. $T_d$ denotes the torque of clutch damper. $T_t$ represents the driving torque of wheels and $T_r$ is the resistant torque.

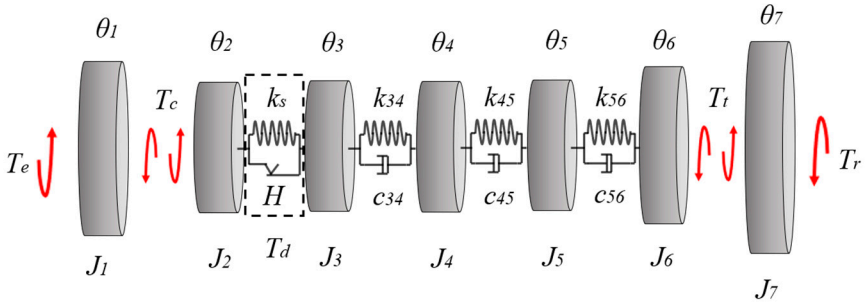


**Figure 1.** Dynamic model of the driveline system for analyzing the torsional vibration.

According to the D'Alembert principle, the differential equations of the model are given as:

$$\mathbf{J}\ddot{\boldsymbol{\theta}} + \mathbf{C}\dot{\boldsymbol{\theta}} + \mathbf{K}\boldsymbol{\theta} = \mathbf{T} \tag{1}$$

where **J**, **C**, **K**, θ and **T** are inertia matrix, damping matrix, stiffness matrix, angular displacement vector and torque vector, respectively. They are expressed as follows:

$$\mathbf{J} = \begin{bmatrix} J_1 & 0 & 0 & 0 & 0 & 0 & 0 \\ 0 & J_2 & 0 & 0 & 0 & 0 & 0 \\ 0 & 0 & J_3 & 0 & 0 & 0 & 0 \\ 0 & 0 & 0 & J_4 & 0 & 0 & 0 \\ 0 & 0 & 0 & 0 & J_5 & 0 & 0 \\ 0 & 0 & 0 & 0 & 0 & J_6 & 0 \\ 0 & 0 & 0 & 0 & 0 & 0 & J_7 \end{bmatrix}, \mathbf{C} = \begin{bmatrix} 0 & 0 & 0 & 0 & 0 & 0 & 0 \\ 0 & 0 & 0 & 0 & 0 & 0 & 0 \\ 0 & 0 & c_{34} & -c_{34} & 0 & 0 & 0 \\ 0 & 0 & -c_{34} & c_{34}+c_{45} & -c_{45} & 0 & 0 \\ 0 & 0 & 0 & -c_{45} & c_{45}+c_{56} & -c_{56} & 0 \\ 0 & 0 & 0 & 0 & -c_{56} & c_{56} & 0 \\ 0 & 0 & 0 & 0 & 0 & 0 & 0 \end{bmatrix},$$

$$\mathbf{K} = \begin{bmatrix} 0 & 0 & 0 & 0 & 0 & 0 & 0 \\ 0 & 0 & 0 & 0 & 0 & 0 & 0 \\ 0 & 0 & k_{34} & -k_{34} & 0 & 0 & 0 \\ 0 & 0 & -k_{34} & k_{34}+k_{45} & -k_{45} & 0 & 0 \\ 0 & 0 & 0 & -k_{45} & k_{45}+k_{56} & -k_{56} & 0 \\ 0 & 0 & 0 & 0 & -k_{56} & k_{56} & 0 \\ 0 & 0 & 0 & 0 & 0 & 0 & 0 \end{bmatrix}, \boldsymbol{\theta} = \begin{bmatrix} \theta_1 \\ \theta_2 \\ \theta_3 \\ \theta_4 \\ \theta_5 \\ \theta_6 \\ \theta_7 \end{bmatrix}, \mathbf{T} = \begin{bmatrix} T_e - T_c \\ T_c - T_d \\ T_d \\ 0 \\ 0 \\ -T_t \\ T_t - T_r \end{bmatrix}.$$

### *2.2. Transient Engine Torque*

As the power source of the drivetrain, the output torque of the engine is primarily composed of gas torque, inertia torque and friction torque. Figure 2a illustrates the motion of crank-link mechanism and the applied loads. Taking the top dead point as the coordinate origin, the displacement of piston $x_p$ is derived as:

$$x_p = r[(1 - \cos\alpha) + 1/\lambda(1 - \cos\beta)] \tag{2}$$

$$\beta = \arcsin(\lambda \sin\alpha) \tag{3}$$

where $r$ is the crank radius, $l$ is the connecting rod length, $\lambda = r/l$ is a scale factor, $\alpha$ is the crankshaft angle and $\beta$ is the intersection angle between connecting rod and cylinder longitudinal axis. Considering the McLaughlin expansion, the velocity $\dot{x}_p$ and acceleration $\ddot{x}_p$ of piston can be expressed as:

$$\dot{x}_p = r\omega(\sin\omega t + \lambda/2 \sin 2\omega t) \tag{4}$$

$$\ddot{x}_p = r\omega^2(\cos\omega t + \lambda \cos 2\omega t) \tag{5}$$

where $\omega$ is the angular velocity of crankshaft. The gas force $F_{eg}$ and the inertia force $F_{ei}$ applied to piston are:

$$F_{eg} = \frac{\pi D^2}{4} P_g \tag{6}$$

$$F_{ei} = -m_i r\omega^2(\cos\omega t + \lambda \cos 2\omega t) \tag{7}$$

where $D$ is the internal diameter of cylinder, $P_g$ is the gas pressure inside the cylinder, and $m_i$ is the translational mass of piston and connecting rod. Utilizing Equations (2)–(7), the gas torque $T_{eg}$ and the inertia torque $T_{ei}$ of one cylinder are given as:

$$T_{eg} = F_{eg} r \sin(\alpha + \beta) / \cos\beta \tag{8}$$

$$T_{ei} = F_{ei} r \sin(\alpha + \beta) / \cos\beta \tag{9}$$

The friction torque of engine is complicated and consisting of multiple items. Here, it is calculated by the Rezeka–Henein [15,16] method, and the equation is given as:

$$T_{ef} = -\left(T_{f1} + T_{f2} + T_{f3} + T_{f4} + T_{f5} + T_{f6}\right) \tag{10}$$

where $T_{f1}$ is the ring viscous lubrication friction torque, $T_{f2}$ is the ring mixed lubrication friction torque, $T_{f3}$ is the piston skirt friction torque, $T_{f4}$ is the valve train friction torque, $T_{f5}$ is the auxiliaries and unloaded bearing friction torque and $T_{f6}$ is the loaded bearing friction torque. They are expressed as:

$$T_{f1} = a_1 \left[\mu(r\omega|K|)\left(P_e + P_g\right)w_0\right]^{0.5} D(n_0 + 0.4n_c) r|K| \tag{11}$$

$$T_{f2} = a_2 \pi D n_c w_c \left(P_e + P_g\right)(1 - |\sin\alpha|) r|K| \tag{12}$$

$$T_{f3} = a_3 \mu \frac{\omega r K}{h_o} D L_s r|K| \tag{13}$$

$$T_{f4} = a_4 n_v F_s r|K| / \sqrt{\omega} \tag{14}$$

$$T_{f5} = a_5 \mu\omega \tag{15}$$

$$T_{f6} = a_6 \frac{\pi D^2}{4} r_c P_g |\cos\alpha| / \sqrt{\omega} \tag{16}$$

$$K = \sin\alpha + \lambda \sin\alpha \cos\alpha / \sqrt{1 - (\lambda \sin\alpha)^2} \tag{17}$$

where $a_i (i = 1, 2, \ldots, 6)$ are the fitting coefficients, $\mu$ is the oil-film viscosity, $P_e$ is the contact pressure of the oil ring, $w_0$ is the oil ring width, $n_0$ is the number of oil rings, $w_c$ is the compressing ring width, $n_c$ is the number of the compressing rings, $h_o$ is the oil-film thickness, $L_s$ is the piston skirt length, $n_v$ is the number of valves of one cylinder, $F_s$ is the valve spring load and $r_c$ is the average radius of journal bearings.

Figure 2b displays the calculated torque of one cylinder when the engine is at idle speed (750 rpm). Summarizing the gas, inertia and friction torques of each cylinder, the total output torque of a four-cylinder/four-stroke engine $T_e$ can be derived as:

$$T_e = \sum_{j=1}^{4} \left(T_{eg(j)} + T_{ei(j)} + T_{ef(j)}\right) \tag{18}$$

where $j$ represents the $j^{th}$ cylinder.

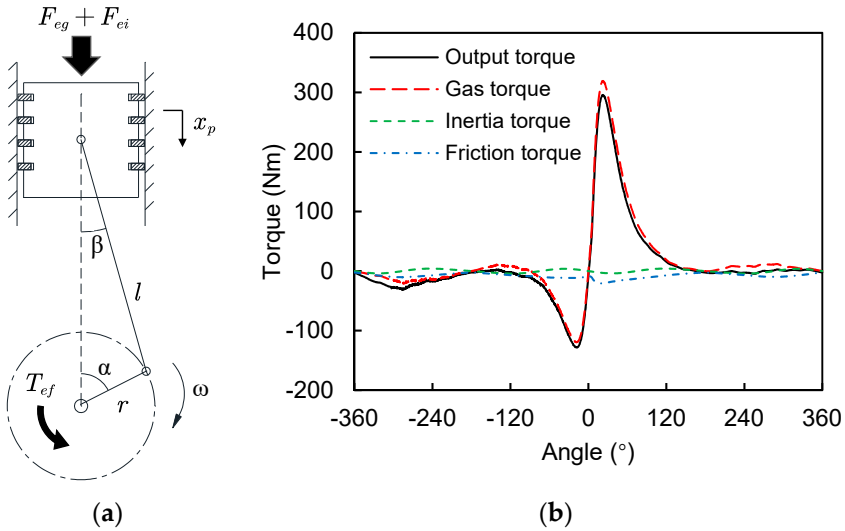


**Figure 2.** Transient model of engine. (**a**) Loads and motion of piston and crank−link mechanism; (**b**) transient torque of one cylinder at 750 rpm.

### *2.3. Nonlinear Clutch Model*

#### 2.3.1. Clutch Friction Model

Figure 3 shows the structure of the multi-stage clutch. When the clutch is engaged, the friction plate is pressed by press plates of clutch driving part, and the power of the engine is transmitted to downstream driveline through friction torque. The engaged clutch may switch in stick or slip states in practice, which depends on the value of the transmitting torque. In stick state, the maximum torque the clutch can transmit $T_{st}$ is given as:

$$T_{st} = \mu_0 N_s R_m F \tag{19}$$

where $\mu_0$ is the static friction coefficient, $N_s$ is the number of friction surfaces, $F$ is the pressing force and $R_m$ is the equivalent friction radius, which can be determined by the clutch inner radius $r_i$ and outer radius $r_o$:

$$R_m = \frac{2\left(r_o^3 - r_i^3\right)}{3\left(r_o^2 - r_i^2\right)} \tag{20}$$

When the driving and driven parts of the clutch rotate relatively, the clutch turns to the slip state. The maximum sliding torque $T_{sl}$ can be derived by replacing the static friction coefficient $\mu_0$ with the dynamic friction coefficient $\mu_s$ in Eq. (19). Then, the stick-slip model of the clutch is expressed as [14]:

$$T_c = \begin{cases} T_{sl} sign\left(\dot{\theta}_1 - \dot{\theta}_2\right) & if \left|\dot{\theta}_1 - \dot{\theta}_2\right| \geq \varepsilon_{tol} \\ T_{st} sign\left(T_p\right) & if \left|\dot{\theta}_1 - \dot{\theta}_2\right| < \varepsilon_{tol}, \left|T_p\right| \geq T_{st} \\ T_p & if \left|\dot{\theta}_1 - \dot{\theta}_2\right| < \varepsilon_{tol}, \left|T_p\right| < T_{st} \end{cases} \tag{21}$$

where $\varepsilon_{tol}$ is a small tolerance value, which is designed to define the operation states of clutch in case of simulation instability. In Equation (21), the transmitting torque $T_p$ can be expressed as Equation (22) or Equation (23):

$$T_{p1(n)} = -J_1 \ddot{\theta}_{1(n-1)} + T_{e(n)} \tag{22}$$

$$T_{p2(n)} = J_2 \ddot{\theta}_{2(n-1)} + T_{d(n)} \tag{23}$$

where the subscripts $n$ and $(n-1)$ represent the $n^{th}$ and $(n-1)^{th}$ numerical calculation step, respectively. In theory, the values of $T_p$ obtained by Equations (22) and (23) should be the same, but actually there is a slight difference between them because of the numerical calculation errors. In order to alleviate the errors, the average value of Equations (22) and (23) will be perceived as the calculated value of $T_p$, and that is:

$$T_{p(n)} = \left(T_{p1(n)} + T_{p2(n)}\right)/2 \tag{24}$$

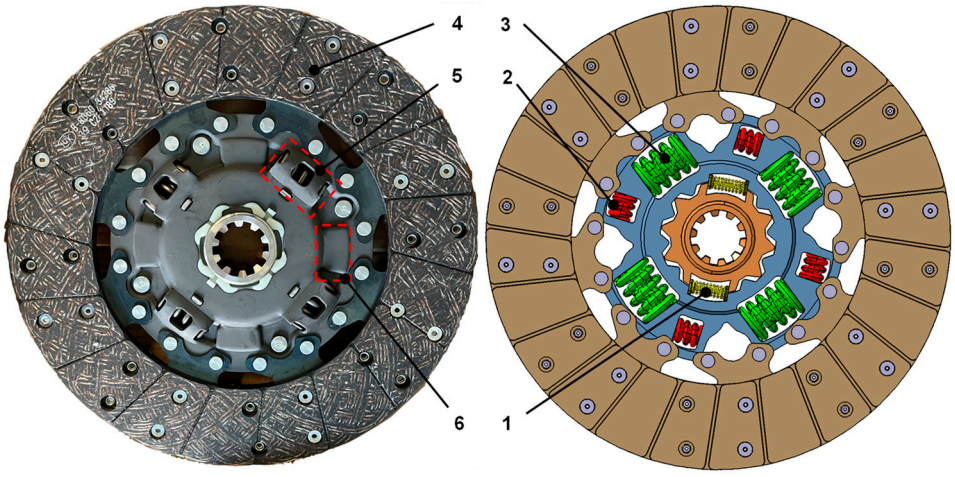


**Figure 3.** Structure of the three-stage clutch. (1. First stage spring; 2. Third stage spring; 3. Second stage spring; 4. Friction plate; 5. Spring window of second stage spring; 6. Spring window of third stage spring.)

#### 2.3.2. Model of the Multi-Stage Clutch Damper

As shown in Figure 3, there are three stages of springs in the clutch damper which form three stages of stiffness of the clutch, and the multi-stage hysteresis torque is formed by damping plates inside the clutch hub. The nonlinear torsional characteristics of a three-stage clutch damper in terms of the transmission torque $T_d$ versus the relative angle $\delta(\delta = \theta_2 - \theta_3)$ can be expressed as piecewise-linear functions, as shown in Figure 4. The torque transmitted through the clutch damper consists of the spring torque $T_S$ and the friction torque $T_H$. They are given as [11,12,25,26]:

$$T_d = T_S + T_H \tag{25}$$

$$T_S = \begin{cases} k_{s1}\Phi_{p1} + k_{s2}(\Phi_{p2} - \Phi_{p1}) + k_{s3}(\delta - \Phi_{p2}) & \delta > \Phi_{p2} \\ k_{s1}\Phi_{p1} + k_{s2}(\delta - \Phi_{p1}) & \Phi_{p1} < \delta \le \Phi_{p2} \\ k_{s1}\delta & -\Phi_{n1} \le \delta \le \Phi_{p1} \\ -k_{s1}\Phi_{n1} + k_{s2}(\delta + \Phi_{n1}) & -\Phi_{n2} \le \delta < -\Phi_{n1} \\ k_{s1}\Phi_{n1} - k_{s2}(\Phi_{n2} - \Phi_{n1}) + k_{s3}(\delta + \Phi_{n2}) & \delta < -\Phi_{n2} \end{cases} \tag{26}$$

$$T_H = \begin{cases} H_1/2 + (H_2 - H_1) + 2/\pi \cdot (H_3 - H_2)\arctan\left(\sigma\dot{\delta}\right) & \dot{\delta} > 0, \delta > \Phi_{p2} \\ H_1/2 + 2/\pi \cdot (H_2 - H_1)\arctan\left(\sigma\dot{\delta}\right) & \dot{\delta} > 0,\ \Phi_{p1} < \delta \le \Phi_{p2} \\ H_1/\pi \cdot \arctan\left(\sigma\dot{\delta}\right) & (\dot{\delta} > 0,\ \delta \le \Phi_{p1}) \,||\, (\dot{\delta} < 0,\ \delta \ge -\Phi_{n1}) \\ -H_1/2 + 2/\pi \cdot (H_2 - H_1)\arctan\left(\sigma\dot{\delta}\right) & \dot{\delta} < 0, -\Phi_{n2} \le \delta < -\Phi_{n1} \\ -H_1/2 - (H_2 - H_1) + 2/\pi \cdot (H_3 - H_2)\arctan\left(\sigma\dot{\delta}\right) & \dot{\delta} < 0, \delta < -\Phi_{n2} \end{cases} \tag{27}$$

where $k_{s1}, k_{s2}$ and $k_{s3}$ are the first, second and third stages of stiffness, respectively, $H_1$, $H_2$,$H_3$ are the first, second and third stages of hysteresis, respectively, $\Phi_{p1}$, $\Phi_{p2}$ are the first and second stage end-stops for the positive side, respectively, and $\Phi_{n1}$, $\Phi_{n2}$ are the

first and second stage end-stops for the negative side, respectively. The item $\arctan\left(\sigma\dot{\delta}\right)$ is the smoothing function for different stages of hysteresis in case of sudden jump and discontinuity when $\dot{\delta}$ is near zero. The value of smoothing index $\sigma$ is set to 500.

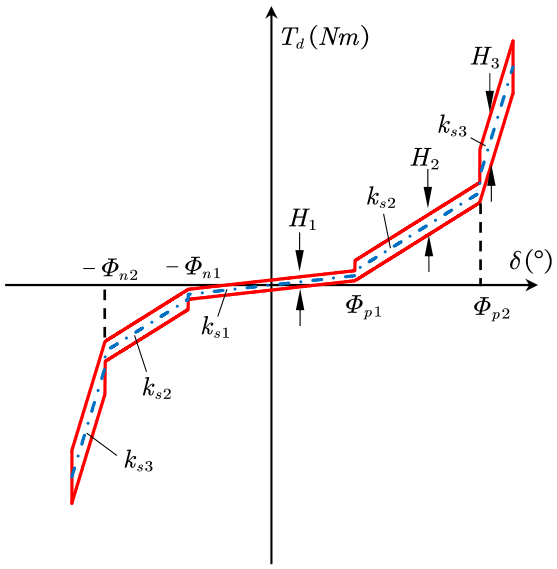


**Figure 4.** The piecewise-linear torsional characteristics of the three-stage clutch damper.

### *2.4. Tire Slip Model*

The fixed relaxation length model mentioned by Bartram [17] is adopted to describe tire slip behavior. In this transient model, the driving torque of the tire $T_t$ has a linear correlation with the localized slip ratio $\kappa_t$ at the contact patch, expressed as:

$$T_t = C_{Fx}\kappa_t R_w \tag{28}$$

where $C_{Fx}$ is the slip stiffness of tire, and $R_w$ is the rolling radius of driving wheel. The localized slip ratio $\kappa_t$ is established as the first order lagging of slip rate $s_w$, given as:

$$S_x\dot{\kappa}_t + \kappa_t V_b = s_w V_b \tag{29}$$

$$s_w = \frac{\dot{\theta}_6 R_w - V_b}{V_b} \tag{30}$$

where $S_x$ represents the longitudinal tire relaxation length, and $V_b$ represents the translational velocity of the car body.

### *2.5. Resistance Torque*

When a vehicle drives on a flat road, the resistance torque $T_r$ is mainly composed of the rolling resistance of wheels $T_{rr}$ and the aerodynamic resistance $T_{ra}$. It can be expressed as:

$$T_r = T_{rr} + T_{ra} \tag{31}$$

$$T_{rr} = mgfR_w \tag{32}$$

$$T_{ra} = 0.5C_D A\rho V_b^2 R_w \tag{33}$$

$$f = 0.0076 + 0.000056V_b \tag{34}$$

where $m$ is the total mass of the vehicle, $f$ is the rolling resistance coefficient, $C_D$ is the aerodynamic resistance coefficient, $A$ is the windward area and $\rho$ is the air density.

## 3. Experimental Validations of 7DOF Powertrain Model

### *3.1. Experiment Setup*

In order to validate the proposed model, we take a light-loaded commercial vehicle (equipped with a four-cylinder diesel engine and a six-speed manual transmission) as an example to set up the experiment of torsional vibration. Figure 5 illustrates the layout of sensors and the equipment of the experiment. Four magnetic sensors are utilized to measure the angular velocities of flywheel, gearbox input shaft, gearbox output shaft and final drive input shaft. To monitor the sound and vibration in the cabin, a microphone is located beside the driver's right ear and a PCB acceleration sensor is mounted on the driver's seat rail. The experiment is conducted under the fourth gear WOT (wide-open throttle) condition. The statistics during vehicle accelerating from 900 rpm to 3000 rpm are collected by LMS SCADAS system and processed in the software Testlab 18. The sampling frequency for velocity and noise signals is 51,200 Hz, and for vibration signals it is 2048 Hz.

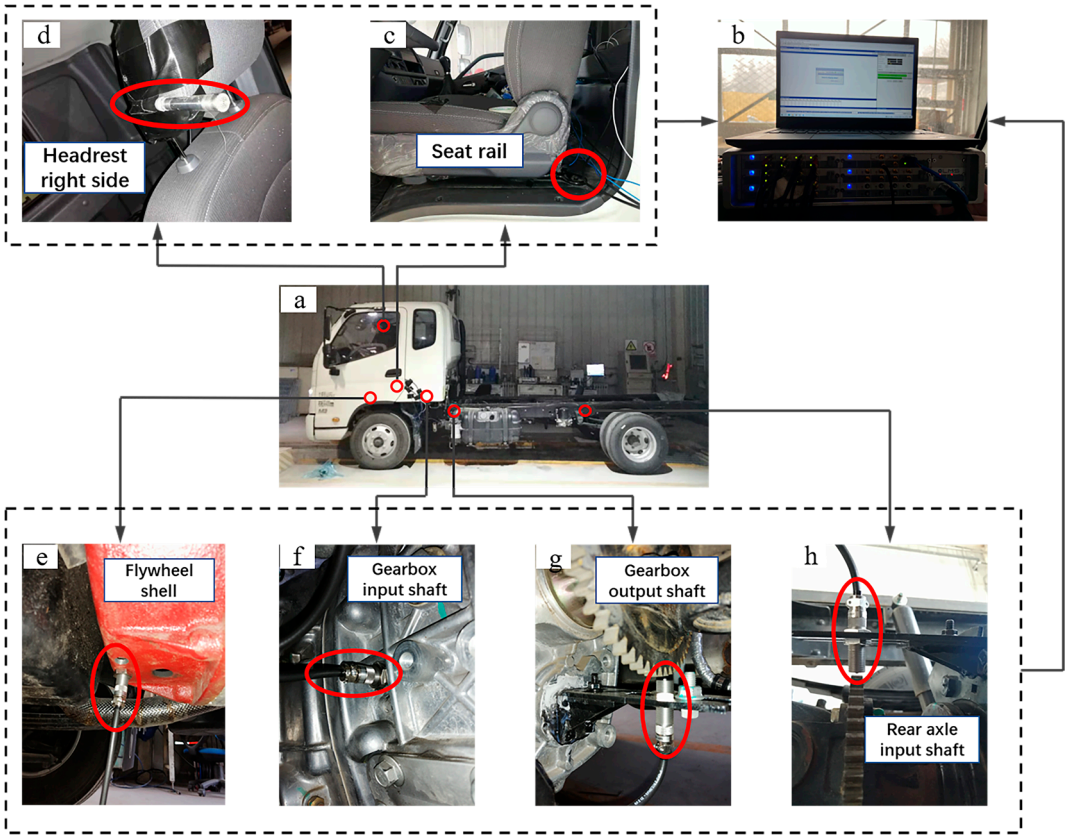


**Figure 5.** Layout of sensors and equipment in the experiment. (**a**) Tested vehicle; (**b**) laptop and LMS SCADAS system; (**c**) acceleration sensor; (**d**) microphone; (**e**–**h**) magnetic sensors for measuring speed.

### *3.2. Model Validation*

Based on the proposed model, a numerical simulation is performed with the R-K method. The model parameters are listed in the Appendix A. Table A1. Figure 6 shows the measured and the calculated results in time domain. It is shown in Figure 6a that the measured velocities of the gearbox input shaft, gearbox output shaft and final drive input shaft undergo strong fluctuations at 4–6 s, which indicates torsional resonance occurs at the downstream driveline during vehicle accelerating. The calculated results in Figure 6b show the same accelerating tendency and speed fluctuating phenomenon as the experimental data. The relative velocities through the clutch damper are shown in Figure 7a. It is seen that the numerical results coincide well with the measured results in the resonance region. By performing STFT (short time Fourier transform) to the velocity data, the second-order speed fluctuation of the gearbox input shaft versus engine speed is extracted, as shown

in Figure 7b. According to the experimental results, it can be observed that the critical speed of the driveline is 1630 rpm (54.33 Hz), and the peak amplitude of the second-order speed fluctuation is 159.15 rpm. Figure 7b also compares the numerical results with the experimental results. It is seen that the model errors are −1.55% for predicting the critical speed and +6.98% for predicting the peak amplitude, which validates the precision of the proposed model.

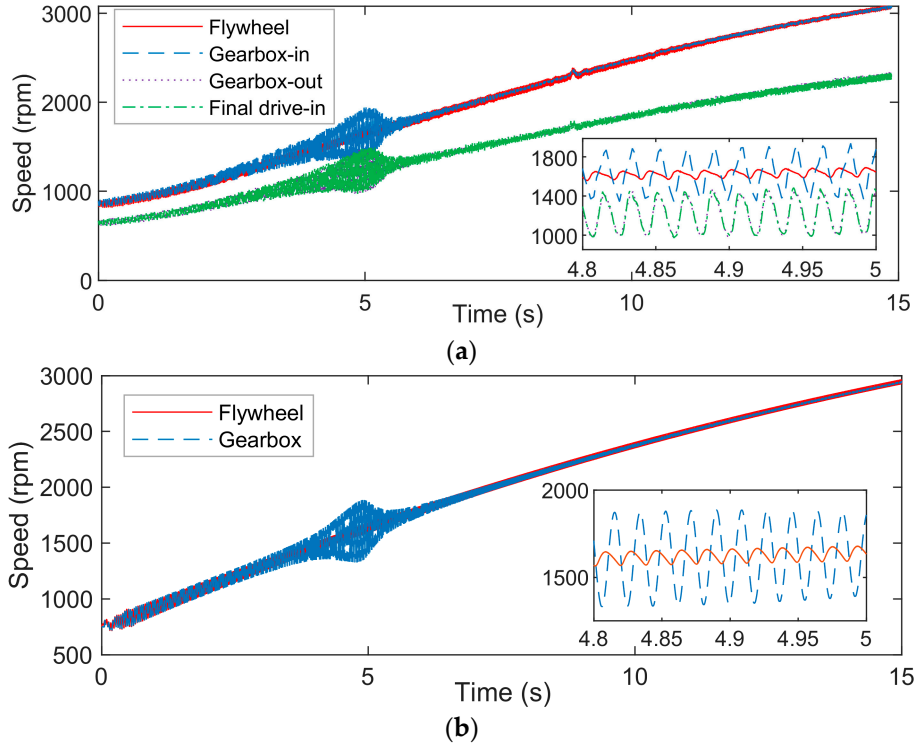


**Figure 6.** Measured and calculated results during vehicle accelerating with the 4th gear. (**a**) Measured speeds of the experiment; (**b**) calculated speeds of the simulation.

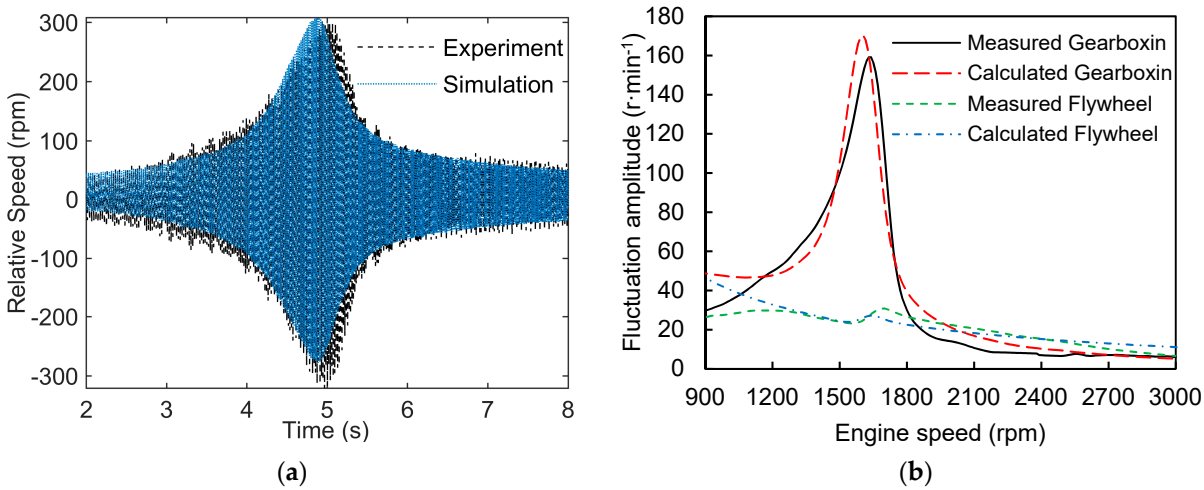


**Figure 7.** Comparisons of the measured and calculated results. (**a**) The relative velocity through the clutch damper; (**b**) the second−order speed fluctuation.

## 4. Natural Characteristics of Driveline System

To obtain the natural characteristics of the driveline system, the driveline model shown in Figure 1 is linearized. The engine inertia $J_1$ and clutch driving part inertia $J_2$ are considered as one whole $J_{12}$. Then, a modal analysis is carried out. The results are

shown in Figure 8. It is seen that the calculated fourth eigenvalue of the driveline (52.92 Hz) corresponds to the measured natural frequency (54.33 Hz), and its modal shape is also consistent with the experimental results.

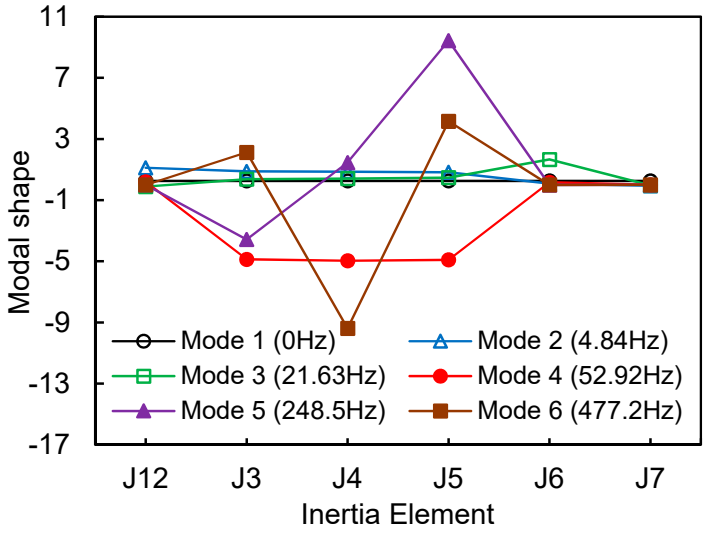


**Figure 8.** Modes of the driveline system.

In order to research the effects of the driveline parameters on the eigenvalue of the driveline, a sensitivity analysis is implemented according to Equation (35), given as [3,27]:

$$\frac{\partial \omega_i}{\partial p_m} = -\frac{1}{2\omega_i}\theta_i^T\left(\omega_i^2\frac{\partial \mathbf{J}}{\partial p_m} - \frac{\partial \mathbf{K}}{\partial p_m}\right)\theta_i \tag{35}$$

where $\omega_i$ represents the $i^{th}$ natural frequency of the system, $p_m$ represents structure parameters and $\theta_i$ is the corresponding eigenvector, which has been regularized with $\theta_i^T\mathbf{J}\theta_i = 1$. According to Equation (35), the sensitivity of $\omega_i$ to the inertia parameter $J_m$ and the stiffness parameter $k_m$ can be expressed as:

$$\frac{\partial \omega_i}{\partial J_m} = -\frac{\omega_i^2\theta_i^T\frac{\partial \mathbf{J}}{\partial J_m}\theta_i}{2\omega_i} = -\frac{\omega_i(\theta_i)_m^2}{2} \tag{36}$$

$$\frac{\partial \omega_i}{\partial k_m} = \frac{\theta_i^T\frac{\partial \mathbf{K}}{\partial k_m}\theta_i}{2\omega_i} = \frac{\left[(\theta_i)_m - (\theta_i)_{m+1}\right]^2}{2\omega_i} \tag{37}$$

where $(\theta_i)_m$ is the $m^{th}$ element of $\theta_i$.

With Equations (36) and (37), the sensitivities of the fourth eigenvalue to the inertia and stiffness parameters are calculated, as shown in Figure 9a. It can be seen that $\omega_4$ is significantly influenced by inertias $J_3$,$J_4$ and $J_5$ with negative correlations and influenced by stiffness parameters $k_{s2}$ and $k_{56}$ with positive correlations. Figure 9b illustrates the variation of $\omega_4$ when the sensitive parameters are adjusted within the manufacturable ranges. It can be seen that the fourth natural frequency varies between 45 Hz and 60 Hz. The influences of sensitive parameters on the eigenvalue are limited, so it is difficult to move the eigenvalue out of the work range of engine (33.3–100 Hz). Therefore, methods for suppressing the driveline oscillation are needed.

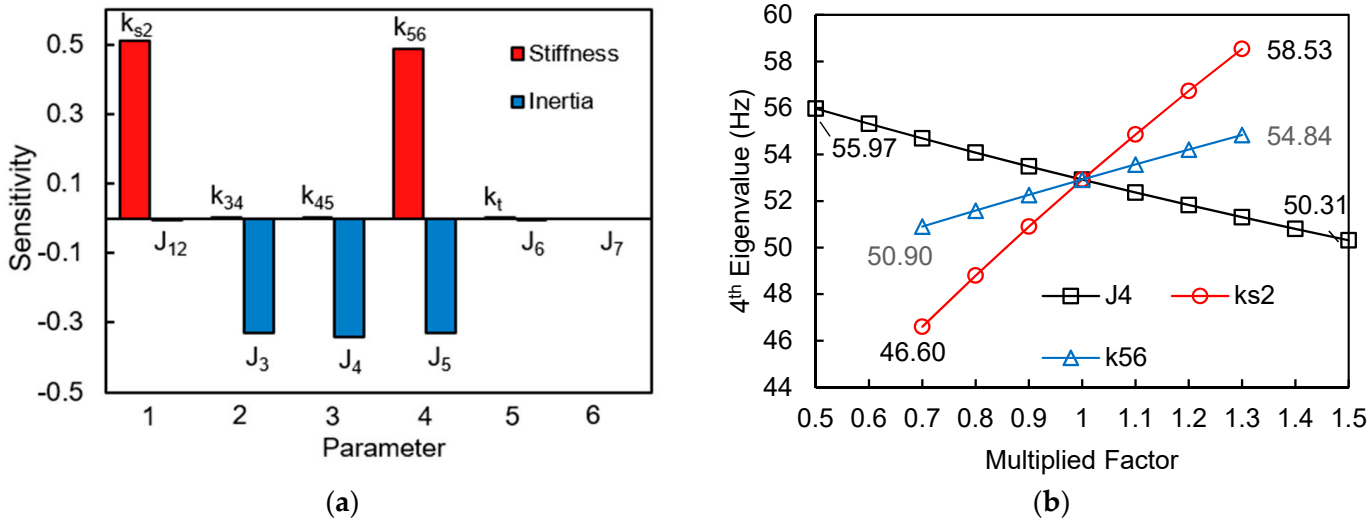


**Figure 9.** Results of sensitivity analysis. (**a**) Sensitivities of the 4th natural frequency; (**b**) influence of sensitive parameters on the 4th natural frequency.

## 5. Influence of Clutch Parameters on the Torsional Vibration

Considering the clutch damper generally works in the main stage (the second stage) during vehicle accelerating, the nonlinear behavior of clutch and the influences of the second stage clutch parameters ($\Phi_{p2}$, $\Phi_{p1}$, $k_{s2}$, $H_2$, $T_{st}$) on the torsional vibration of the driveline are investigated. The second-order speed fluctuation of transmission is considered as a measurement of the driveline torsional vibration.

Figure 10a shows the influence of the second end-stop angle $\Phi_{p2}$ on the torsional vibration of driveline. It indicates that the oscillation amplitude in the resonance region is reduced with the decrease of $\Phi_{p2}$.The nonlinear behaviors of the clutch damper can be observed in the upper envelopes of the relative angle of the clutch damper, as shown in Figure 10b. The envelope curves are calculated with Hilbert transform method [28]. It is seen that the relative angle of the clutch damper does not reach the second end-stop in baseline situation ($\Phi_{p2} = 16^{\circ}$). However, with the decrease of the second end-stop angle, the fluctuated angle starts to cross the transition angle $\Phi_{p2}$ and oscillate between the second and the third stage stiffness regions. Hence, the clutch damper behaves by hardening nonlinear type vibration characteristics, especially when $\Phi_{p2}$ is less than 14°. The envelope curve bends to right side (higher speed side) at the transition angle $\Phi_{p2}$, which results in a decrease of the resonant amplitude and a rise of the critical speed. The smaller $\Phi_{p2}$, the smaller the resonant amplitude and the higher the critical speed.

Figure 11a illustrates the effect of the first end-stop angle $\Phi_{p1}$ on the torsional vibration of drivetrain. It can be seen that the oscillation amplitude in the resonance region is reduced with the increasing of $\Phi_{p1}$, which is similar to the situation when reducing $\Phi_{p2}$. With the increment of the first end-stop angle, the mean angular displacement of the clutch damper is increased, and the hardening type nonlinear vibration of clutch damper occurs, as shown in Figure 11b. The envelope curve bends to the right side at the transition angle $\Phi_{p2}$ (16°), suppressing the resonant amplitude of the driveline.

Figure 12 indicates the influence of the second stage stiffness $k_{s2}$ on the torsional vibration of the drivetrain. It is observed that the oscillation amplitude in the resonance region decreases with the descent of the stiffness since a softer clutch damper can better isolate the torque fluctuation of the engine. It is also seen that the natural frequency becomes higher with the increasing of the stiffness, which is consistent with the analytical results in Section 4.

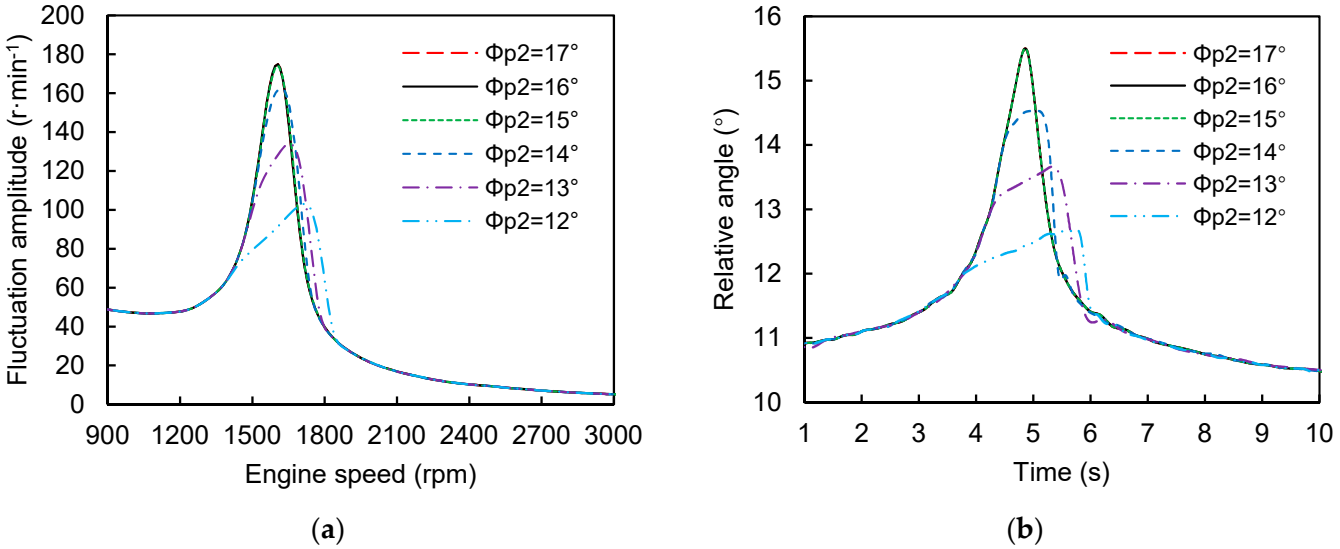


**Figure 10.** Influence of the second end−stop angle $\Phi_{p2}$ on the torsional vibration of driveline. (**a**) Second−order speed fluctuation of transmission; (**b**) upper envelope of the relative angle of the clutch (baseline: the black solid curve).

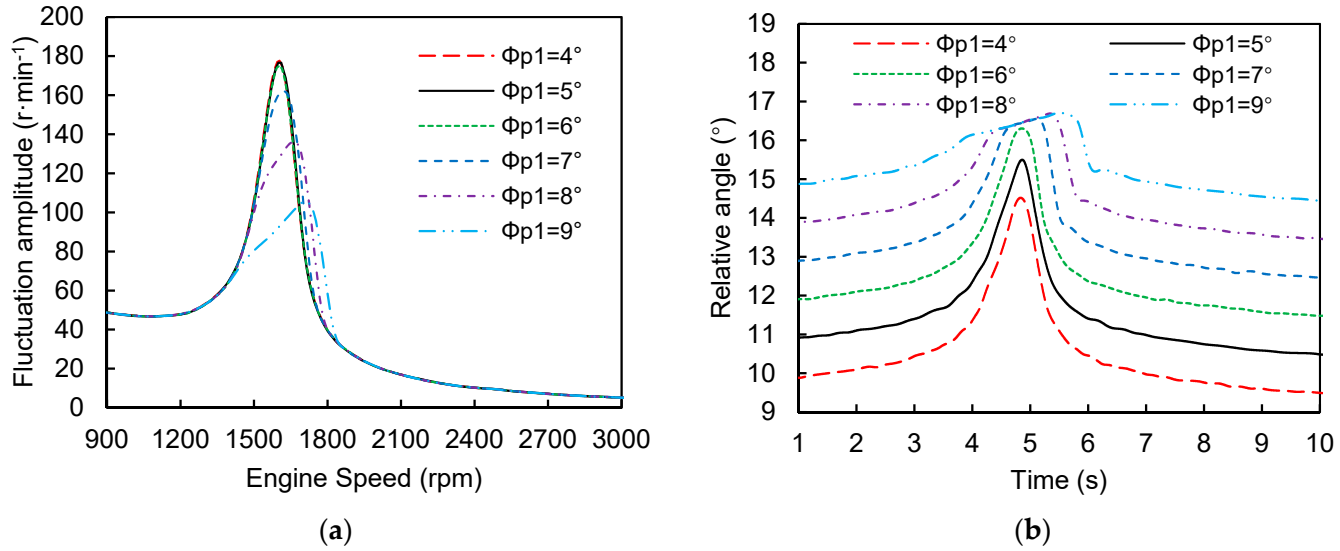


**Figure 11.** Influence of the first end−stop angle $\Phi_{p1}$ on the torsional vibration of driveline. (**a**) Second−order speed fluctuation of transmission; (**b**) upper envelope of the relative angle of the clutch (baseline: the black solid curve).

Figure 13a shows the effect of the hysteresis of second stage $H_2$ on the torsional vibration of drivetrain. It illustrates that the vibration amplitude in the resonant area is gradually mitigated with the increasing of the hysteresis since greater damping can dissipate the vibrational energy within a smaller number of oscillations. However, it can be observed in Figure 13b that the torsional vibration of the driveline is magnified under the high frequency excitation of the engine when the hysteresis of the clutch increases.

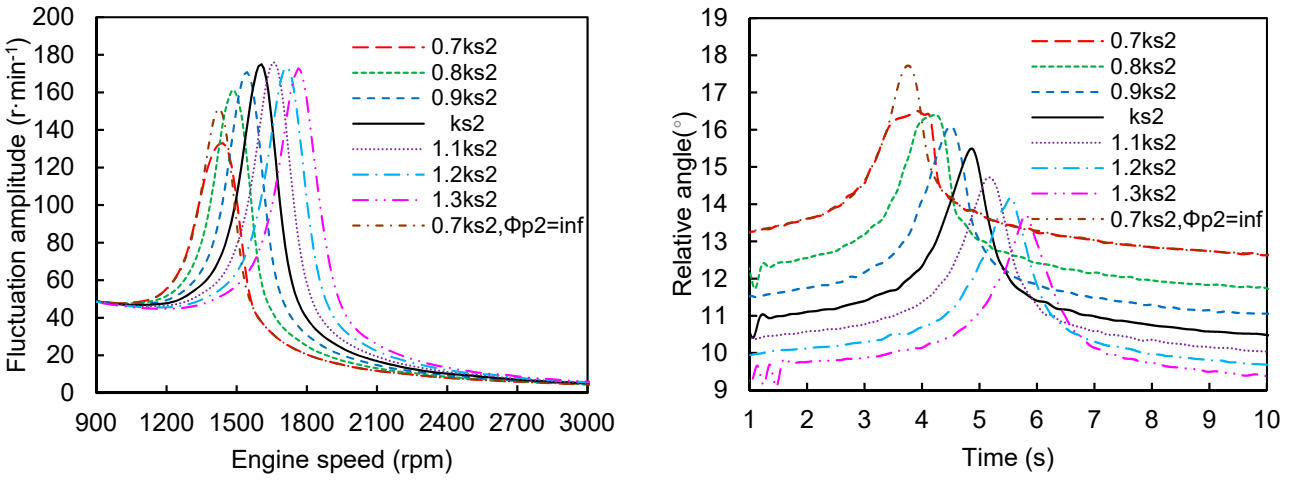


**Figure 12.** Influence of the second stage stiffness $k_{s2}$ on the torsional vibration of driveline. (**a**) Second−order speed fluctuation of transmission; (**b**) upper envelope of the relative angle of the clutch (baseline: the black solid curve).

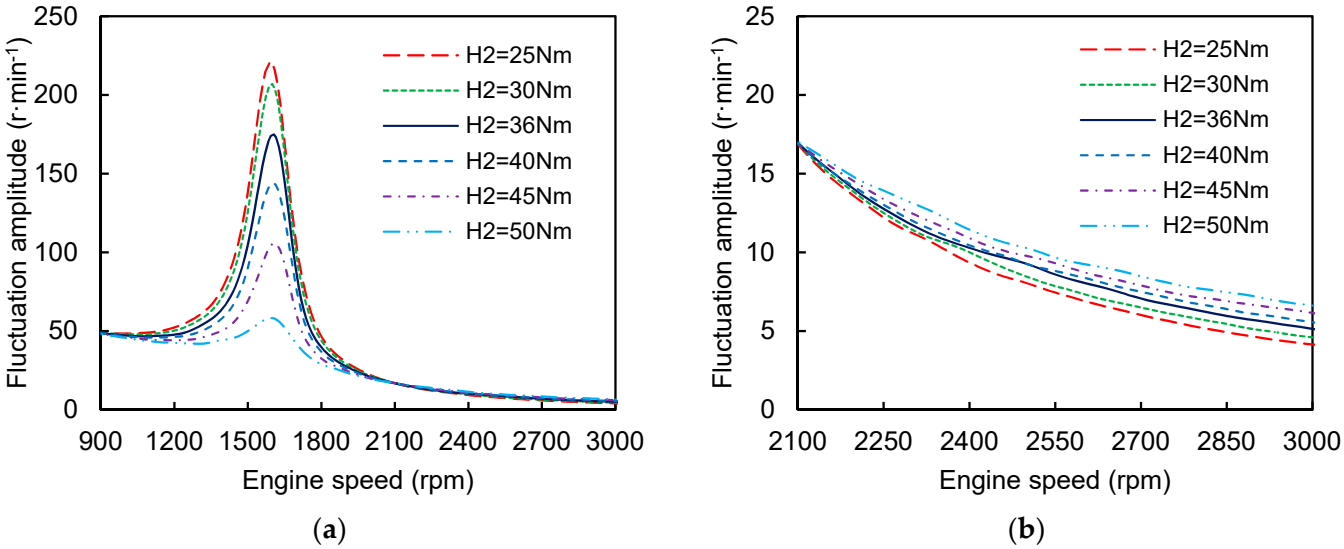


**Figure 13.** Influence of the second stage hysteresis $H_2$ on the torsional vibration of driveline. (**a**) Second−order speed fluctuation of transmission; (**b**) partial enlarged view (baseline: the black solid curve).

Figure 14 indicates the influence of the maximum friction of the clutch $T_{st}$ on the torsional vibration of drivetrain. It can be seen that the maximum friction influences the vibration amplitude at the critical speed, and the peak value is slightly increased with the increasing of the maximum friction. Additionally, the variation of the maximum friction has almost no impact on the powertrain vibration at other speeds.

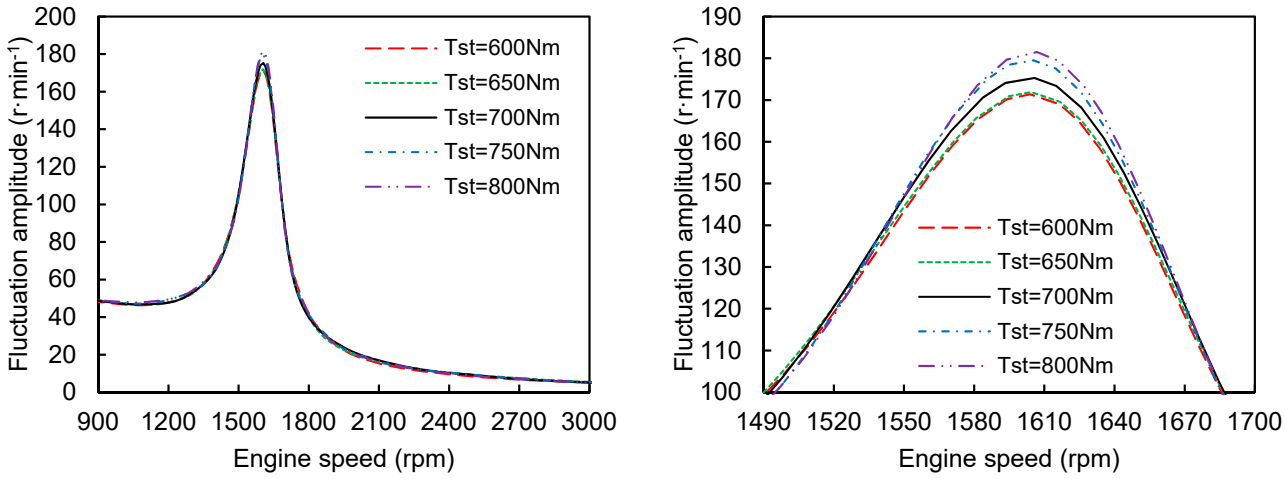


**Figure 14.** Influence of the maximum friction $T_{st}$ on the torsional vibration of driveline. (**a**) Second−order speed fluctuation of transmission; (**b**) partial enlarged view (baseline: the black solid curve).

## 6. Applications

### *6.1. Design of an Optimized Clutch*

According to the analyzed results in Section 5, the clutch parameters have significant influence on the torsional vibration of the drivetrain system. In order to evaluate the effectiveness of the nonlinear vibration characteristics of the clutch on attenuating driveline resonance, we take the tested vehicle as an example to optimize the clutch parameters. Considering the preservation of the isolation performances of the clutch under idle conditions and high-speed conditions, the optimization problem is finally determined as follows:

$$\begin{cases} \text{Min} & \Psi\left(k_{\text{s2}}, \Phi_{\text{p2}}\right) \\ s.t. & k_{\text{s2min}} \le k_{\text{s2}} \le k_{\text{s2max}} \\ & \Phi_{\text{p2min}} \le \Phi_{\text{p2}} \le \Phi_{\text{p2max}} \end{cases} \tag{38}$$

where the objective function Ψ is the peak value of the second-order speed fluctuation of the gearbox.

A GA (genetic algorithm) program is developed and co-simulated with the dynamic model to find out the optimal solution. In the program, the population size is set to 30. The selection method is Roulette and the crossover method is single-point. The rates of crossover and mutation are 0.8 and 0.005, respectively. The GA program is run more than 10 times and the result converges well after 60 iterations on average. The optimized clutch parameters are shown in Table 1. The calculated amplitude–frequency response and the second-order torsional vibration of the modified drivetrain system are shown in Figure 15. It is seen that the resonant amplitude is obviously reduced after optimization. The critical speed (1668 rpm, 55.60 Hz) is higher than the calculated eigenvalue with the optimized $k_{s2}$ (47.71 Hz) because of the hardening type nonlinear vibration of the clutch damper, which is consistent with the analytical results in Section 5.

**Table 1.** Optimized clutch parameters.

| Parameters | Baseline | Optimized | Manufactured |
|---|---|---|---|
| Second stiffness $k_{s2}$ (Nm/°) | 56 | 42 | 40.6 |
| Second end-stop $\Phi_{p2}$ (°) | 16 | 13 | 12.9 |

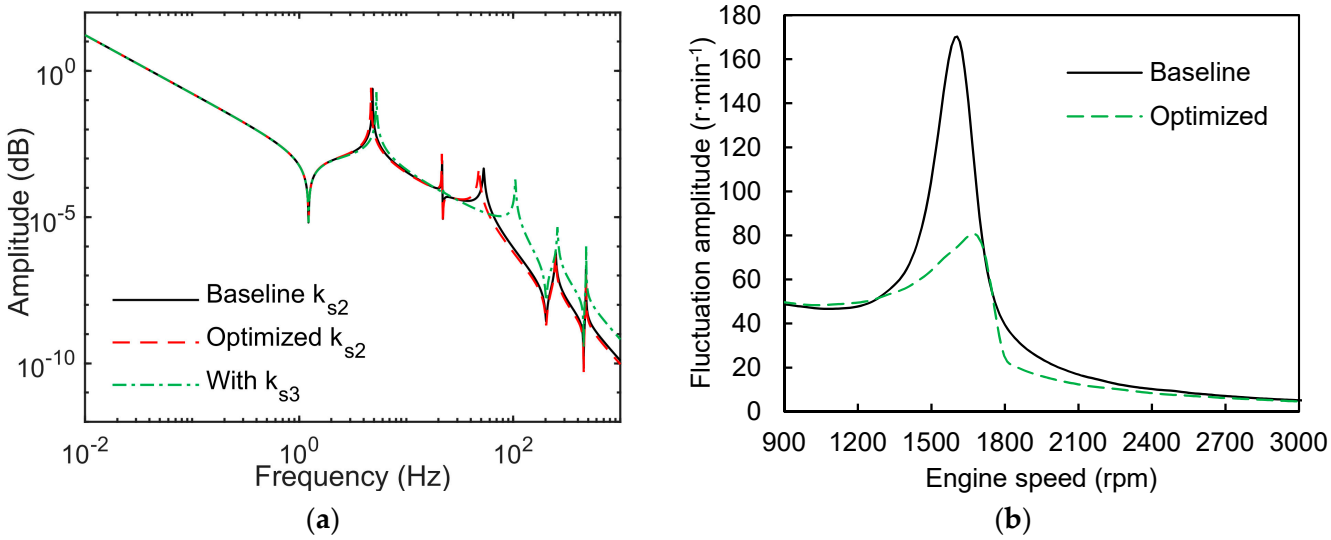


**Figure 15.** Calculated results of the optimized clutch. (**a**) Frequency response function of transmission; (**b**) the second−order speed fluctuation of transmission.

### *6.2. Measurement of the Optimized Clutch*

In order to validate the analytical results, a revised clutch based on the optimized parameters is manufactured by adjusting the coil spring stiffness of the main stage and the circumferential position of the spring windows. The optimized clutch is tested on the vehicle under the fourth gear WOT condition as before.

The measured results are shown in Figure 16. It can be seen from Figure 16a that the speed fluctuation of driveline is greatly mitigated with the revised clutch. It is shown in Figure 16b that the second-order torsional vibration of the gearbox decreases by 42.28% (from 159.15 r·min$^{-1}$ to 91.86 r·min$^{-1}$), and the critical speed locates at a higher speed (1748 rpm, 58.27 Hz), as expected, because of the hardening type nonlinear vibration of the clutch damper. As the torsional vibration of driveline is mitigated, the noise and vibration in the cabin are also reduced, and the driving comfort is greatly improved, as shown in Figure 16c. The experimental results above validate the analytical results presented in this study.

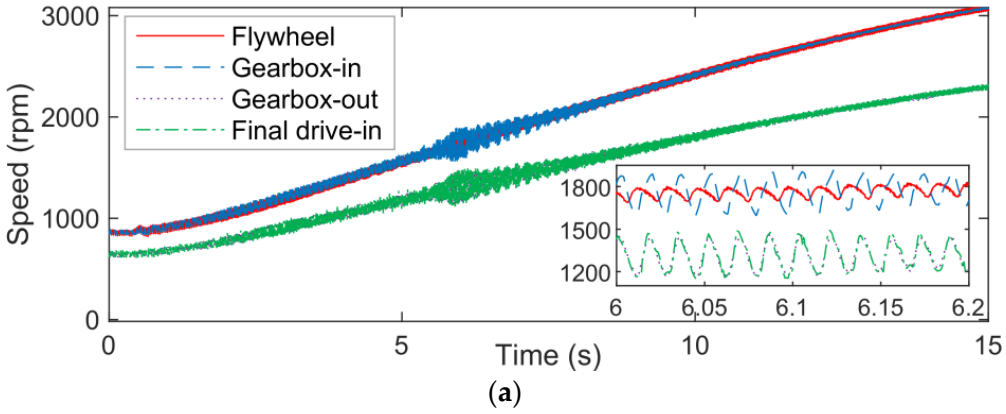


**Figure 16.** *Cont.*

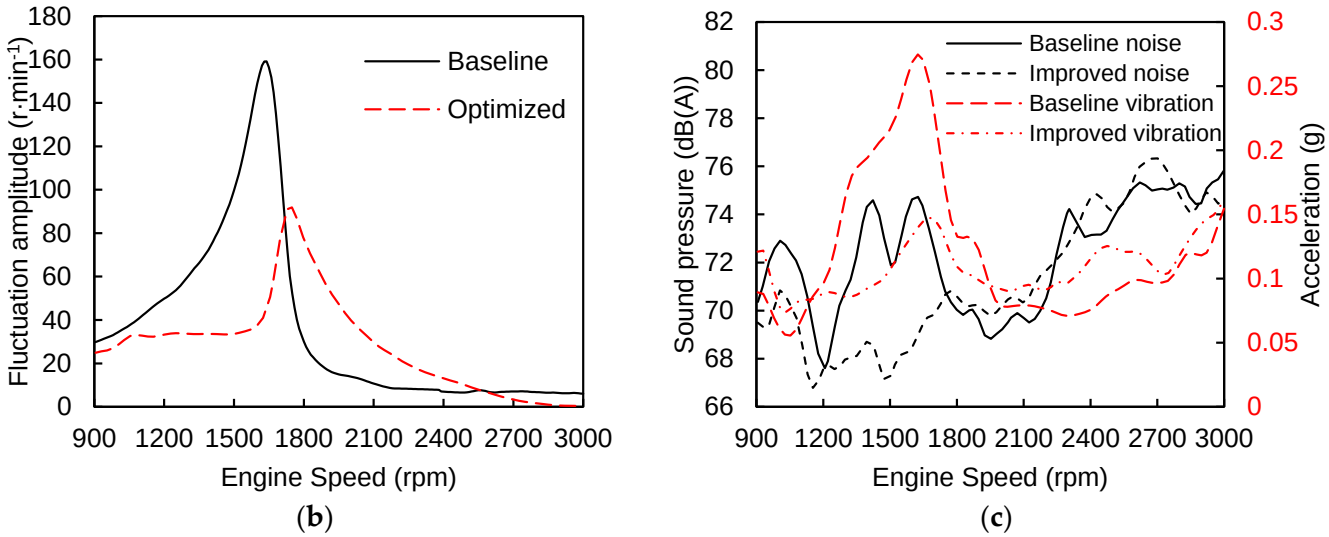


**Figure 16.** Measured results of the optimized clutch. (**a**) Speeds of the revised clutch; (**b**) the second−order speed fluctuation of transmission; (**c**) noise and vibration in the cabin.

## 7. Conclusions

(1) This article proposes a 7 DOF nonlinear model of powertrain system, considering transient engine torque, nonlinear characteristics of multi-stage clutch and tire slip. Taking a generic driveline of a light-loaded commercial vehicle as an example, the dynamic responses of driveline are calculated with numerical methods based on the proposed model. On the real vehicle, an experiment of torsional vibration is conducted under the fourth gear WOT condition. The experimental results validate the precision of the proposed model.

(2) The clutch parameters have significant influence on the driveline torsional vibration. A decrease of the second stage stiffness $k_{s2}$ or an increase of the second stage hysteresis $H_2$ will reduce the second order speed fluctuation of driveline. Increasing the first end-stop angle $\Phi_{p1}$ or reducing the second end-stop angle $\Phi_{p2}$ can mitigate the torsional resonance amplitude of driveline due to the hardening type nonlinear behavior of the clutch damper. Based on the nonlinear vibration characteristics of the clutch damper, an optimized clutch is designed and tested on the vehicle. The numerical and experimental results demonstrate the analytical results in this study.

**Author Contributions:** Methodology, J.Q. and W.S.; software, J.Q.; validation, J.Q., J.W. and Z.C.; resources, J.W.; writing—original draft preparation, J.Q.; writing—review and editing, W.S. and Z.C.; funding acquisition, Z.C. and W.S. All authors have read and agreed to the published version of the manuscript.

**Funding:** This research was funded by the National Key Research and Development Plan of China (2018YFB0106203).

**Data Availability Statement:** Not applicable.

**Conflicts of Interest:** The author(s) declare no potential conflict of interest with respect to the research, authorship, and/or publication of this article.

## Appendix A. Variables and Values

**Table A1. Variables and Values of dynamic model.**

| Variable | Value | Variable | Value | Variable | Value |
|---|---|---|---|---|---|
| $J_1$ (kg·m$^2$) | $7.14 \times 10^{-1}$ | $a_3$ | 0.05 | $R_m$ (mm) | 124.6 |
| $J_2$ (kg·m$^2$) | $1.9 \times 10^{-2}$ | $a_4$ | 1 | $\mu_0$ | 0.28 |
| $J_3$ (kg·m$^2$) | $2.38 \times 10^{-2}$ | $a_5$ | 2 | $k_{s1}$ (Nm/°) | 0.5 |
| $J_4$ (kg·m$^2$) | $8.63 \times 10^{-3}$ | $a_6$ | 0.05 | $k_{s2}$ (Nm/°) | 56 |
| $J_5$ (kg·m$^2$) | $7.62 \times 10^{-3}$ | $\mu$ (kg·m$^{-1}$·s$^{-1}$) | 0.015 | $k_{s3}$ (Nm/°) | 291 |
| $J_6$ (kg·m$^2$) | $3.49 \times 10^{-1}$ | $P_e$ (kPa) | 20 | $H_1$ (Nm) | 4 |
| $J_7$ (kg·m$^2$) | 13.96 | $w_0$ (mm) | 6 | $H_2$ (Nm) | 36 |
| $k_{34}$ (Nm·rad$^{-1}$) | $3.89 \times 10^5$ | $n_0$ | 2 | $H_3$ (Nm) | 94 |
| $k_{45}$ (Nm·rad$^{-1}$) | $2.07 \times 10^5$ | $n_c$ | 3 | $\Phi_{p1}$ (°) | 5 |
| $k_{56}$ (Nm·rad$^{-1}$) | $1.07 \times 10^3$ | $w_c$ (mm) | 4 | $\Phi_{p2}$ (°) | 16 |
| $c_{34}$ (Nm·s·rad$^{-1}$) | 0.01 | $h_o$ (m) | $2 \times 10^{-6}$ | $\Phi_{n1}$ (°) | 5 |
| $c_{45}$ (Nm·s·rad$^{-1}$) | 0.01 | $L_s$ (m) | 0.15 | $\Phi_{n2}$ (°) | 12 |
| $c_{56}$ (Nm·s·rad$^{-1}$) | 0.25 | $n_v$ | 2 | $C_{Fx}$ (N) | $8 \times 10^4$ |
| $r$ (mm) | 51 | $F_s$ (N) | 300 | $R_w$ (m) | 0.376 |
| $l$ (mm) | 155.5 | $r_c$ (m) | 0.06 | $S_x$ (m) | 0.6 |
| $D$ (mm) | 104 | $N_s$ | 2 | $m$ (kg) | 3450 |
| $m_i$ (kg) | 0.45 | $F$ (N) | $1 \times 10^4$ | $C_D$ | 0.7 |
| $a_1$ | 32 | $r_i$ (mm) | 95 | $A$ (m$^2$) | 4.1 |
| $a_2$ | 0.05 | $r_o$ (mm) | 150 | $\rho$ (N·s$^2$·m$^{-4}$) | 1.2258 |

## References


1. Wang, Y.; Qin, X.; Huang, S.; Deng, S. Design and analysis of a multi-stage torsional stiffness dual mass flywheel based on vibration control. *Appl. Acoust.* **2016**, *104*, 172–181. [CrossRef]
2. Li, L.H.; Singh, R. Analysis of start-up transient for a powertrain system with a nonlinear clutch damper. *Mech. Syst. Signal Processing* **2015**, *62–63*, 460–479. [CrossRef]
3. Gao, P.; Xiang, C.; Liu, H.; Zhou, H. Reducing variable frequency vibrations in a powertrain system with an adaptive tuned vibration absorber group. *J. Sound Vib.* **2018**, *425*, 82–101. [CrossRef]
4. Castellazzi, L.; Tonoli, A.; Amati, N.; Galliera, E. A study on the role of powertrain system dynamics on vehicle driveability. *Veh. Syst. Dyn.* **2017**, *55*, 1012–1028. [CrossRef]
5. Markert, R.; Seidler, M. Analytically based estimation of the maximum amplitude during passage through resonance. *Int. J. Solids Struct.* **2001**, *38*, 1975–1992. [CrossRef]
6. Li, L.H.; Singh, R. Analysis of vibration amplification in a multi-staged clutch damper during engine start-up. *Proc. Inst. Mech. Eng. Part D J. Automob. Eng.* **2015**, *229*, 1406–1418. [CrossRef]
7. Li, L.H.; Singh, R. Analysis of speed-dependent vibration amplification in a nonlinear driveline system using Hilbert Transform. *SAE Int. J. Passeng. Cars-Mech. Syst.* **2013**, *6*, 1120–1126. [CrossRef]
8. Idehara, S.J.; Flach, F.L.; Lemes, D. Modeling of nonlinear torsional vibration of the automotive powertrain. *J. Vib. Control.* **2018**, *24*, 1774–1786. [CrossRef]
9. Liu, X.-L.; Shangguan, W.-B.; Jing, X.; Ahmed, W. Vibration isolation analysis of clutches based on trouble shooting of vehicle accelerating noise. *J. Sound Vib.* **2016**, *382*, 84–99. [CrossRef]
10. Crowther, A.R.; Zhang, N. Torsional finite elements and nonlinear numerical modelling in vehicle powertrain dynamics. *J. Sound Vib.* **2005**, *284*, 825–849. [CrossRef]
11. Wei, Z.; Shangguan, W.-B.; Liu, X.; Hou, Q. Modeling and analysis of friction clutches with three stages stiffness and damping for reducing gear rattles of unloaded gears at transmission. *J. Sound Vib.* **2020**, *483*, 115469. [CrossRef]
12. Shangguan, W.-B.; Liu, X.-L.; Yin, Y.; Rakheja, S. Modeling of automotive driveline system for reducing gear rattles. *J. Sound Vib.* **2018**, *416*, 136–153. [CrossRef]
13. Yucesan, A.; Sezer, S. Vibration isolation with clutch disk pre-damper mechanism for the idle rattle phenomenon. *J. Vib. Control.* **2018**, *24*, 1518–1534. [CrossRef]
14. Li, L.P.; Lu, Z.J.; Liu, X.L. Modeling and analysis of friction clutch at a driveline for suppressing car starting judder. *J. Sound Vib.* **2018**, *424*, 335–351. [CrossRef]
15. Rezeka, S.F.; Henein, N.A. A new approach to evaluate instantaneous friction and its components in internal combustion engines. *SAE Trans.* **1984**, *93*, 932–944.
16. Wu, H.W.; Wu, G.Q. Driveline torsional analysis and clutch damper optimization for reducing gear rattle. *Shock. Vib.* **2016**, *2016*, 8434625. [CrossRef]

17. Bartram, M.; Mavros, G.; Biggs, S. A study on the effect of road friction on driveline vibrations. *Proc. Inst. Mech. Eng. Part K J. Multi-Body Dyn.* **2010**, *224*, 321–340. [CrossRef]
18. Jurmu, L.; Robinette, D.; Blough, J.; Gehringer, M. Design and test of a torsional vibration absorber in series with a planetary gearset. *J. Vib. Control.* **2021**, *27*, 1498–1510. [CrossRef]
19. Yang, C.; Tan, X.D.; Hua, L. Multi objective optimization of parameters of torsional vibration dampers considering damping effect and light weight design. *Int. J. Veh. Struct. Syst.* **2019**, *11*, 1–6. [CrossRef]
20. Steinel, K. *Clutch Tuning to Optimize Noise and Vibration Behavior in Trucks and Buses*; SAE Technical Paper Series; SAE International: Warrendale, PA. USA, 2000; p. 3292.
21. Chen, L.; Shi, W.K.; Chen, Z.Y. Research on dynamic behavior of torsional absorber in powertrain system considering nonlinear factors. *J. Vib. Control.* **2021**, *27*, 1656–1667.
22. Yoon, J.Y.; Yoon, H.S. Nonlinear frequency response analysis of a multistage clutch damper with multiple nonlinearities. *J. Comput. Nonlinear Dyn.* **2014**, *9*, 031007. [CrossRef]
23. Kim, T.C.; Rook, T.E.; Singh, R. Effect of smoothening functions on the frequency response of an oscillator with clearance non-linearity. *J. Sound Vib.* **2003**, *263*, 665–678. [CrossRef]
24. Ranjbarzadeh, H.; Kakavand, F. Determination of nonlinear vibration of 2DOF system with an asymmetric piecewise-linear compression spring using incremental harmonic balance method. *Eur. J. Mech. A: Solids* **2019**, *73*, 161–168. [CrossRef]
25. Krak, M.; Dreyer, J.; Singh, R. Development of a non-linear clutch damper experiment exhibiting transient dynamics. *SAE Int. J. Passeng. Cars Mech. Syst.* **2015**, *8*, 754–761. [CrossRef]
26. Saleh, A.; Krak, M.; Dreyer, J.; Singh, R. Development of refined clutch-damper subsystem dynamic models suitable for time domain studies. *SAE Int. J. Passeng. Cars Mech. Syst.* **2015**, *8*, 733–741. [CrossRef]
27. Liu, H.; Xiang, C.L.; Zheng, M.Q. Sensitivity analysis and dynamic modification of natural characteristic in vehicle powertrain. *Automot. Eng.* **2003**, *25*, 591–594. (In Chinese)
28. Feldman, L. Hilbert transform in vibration analysis. *Mech. Syst. Signal Processing* **2010**, *25*, 735–802. [CrossRef]